≪Research Paper≫ Applied Science and Convergence Technology Vol.23 No.2, March 2014, pp.90~96
http://dx.doi.org/10.5757/ASCT.2014.23.2.90

Structural and Electrical Properties of ZrO_2 Films Coated onto PET for High-Energy-Density Capacitors

Sangshik Park*

School of Nano Materials Engineering, Kyungpook National University, Gyeongbuk 742-711

(Received March 17, 2014, Revised March 26, 2014, Accepted March 26, 2014)

Flexible ZrO_2 films as dielectric materials for high-energy-density capacitors were deposited on polyethylene terephthalate (PET) substrates by RF magnetron sputtering. The growth behavior, microstructure and electrical properties of the flexible ZrO_2 films were dependent on the sputtering pressure and gas ratio. Although ZrO_2 films were deposited at room temperature, all films showed a tetragonal crystalline structure regardless of the sputtering variables. The surface of the film became a surface with large white particles upon an increase in the O_2/Ar gas ratio. The RMS roughness and crystallite size of the ZrO_2 films increased with an increase in the sputtering pressure. The electrical properties of the ZrO_2 films were affected by the microstructure and roughness. The ZrO_2 films exhibited a dielectric constant of 21~38 at 1 kHz and a leakage current density of 10^{-6}~10^{-5} A/cm^2 at 300 kV/cm.

Keywords : Flexible ZrO_2 film, Sputter, High-energy-density capacitor, Dielectric constant, Leakage current

I. Introduction

High-energy-density capacitors have been used extensively in pulsed power systems for energy storage, power conditioning and filtering. The recent growing requirements for compact and high-energy density power systems stimulate interest in the application of new dielectric materials. Dielectric materials play a key role in power capacitors for charge control and energy storage processes [1,2]. Polymer dielectrics are currently the primary choice of materials for high-energy-density capacitors owing to their relatively high breakdown strength, low dielectric loss and low cost. The polymers in traditional capacitors include polyethylene terephthalate (PET) and polypropylene (PP), among others [3,4] but the low dielectric constant (ε_r~2 to 3) of polymer dielectrics limits their applications. On the other hand, ceramic capacitors have a much higher energy density than polymer film capacitors due to the high dielectric constant of ceramics. However, ceramic capacitors have a low breakdown strength due to microstructural defects, resulting in a low energy density [5,6].

The energy that can be stored in a capacitor depends on the relative dielectric constant and the breakdown strength of the dielectric layer according to equation (1),

$$E = \frac{1}{2} \cdot \varepsilon_0 \cdot \varepsilon_r \cdot E_b^2 \quad (1)$$

* [E-mail] parkss@knu.ac.kr

where E is the energy stored per unit volume (J/m^3), ε_0 is the dielectric constant of a vacuum, ε is the relative dielectric constant of the dielectrics and E_b is the breakdown strength (V/m). The energy density of a capacitor will increase if E_b is kept constant and the ε value is increased.

The aim of this study was to apply a ceramic dielectric film to high-energy-density capacitors with the structure of a polymer film capacitor. In this study, zirconia (ZrO_2) films were deposited on an aluminum metallized PET substrate. ZrO_2 has been evaluated extensively for electronic applications, including memory devices, oxide fuel cells and oxygen sensor [7-9]. Owing to its relatively high dielectric constant, ZrO_2 can be considered a potential dielectric material for high-energy-density capacitor applications. A range of techniques have been used to prepare ZrO_2 thin films, including sputtering [10], chemical vapor deposition [11], pulsed laser deposition [12] and sol-gel techniques [13]. In this study, ZrO_2 films were deposited on flexible PET substrates by RF magnetron sputtering. The applicability of a ZrO_2/PET film to high-energy-density capacitors was evaluated by examining the effects of the sputtering variables on the electrical properties.

II. Experimental Procedures

The flexible ZrO_2 films were deposited on PET substrates at room temperature by RF magnetron sputtering. A ZrO_2 target with a two-inch diameter (Cerac Inc.) was used. The deposition process was performed at a fixed substrate-to-target distance of 60 mm. PET films, 4~10 μm thick, were used as substrates. The base pressure was $< 1\times10^{-6}$ Torr and sputtering was carried out in an Ar atmosphere. An RF power of 200 W was applied to the target, and ZrO_2 films were deposited on PET and Al/PET substrates. ZrO_2 films were prepared at different sputtering pressures and $Ar:O_2$ gas ratios as a sputtering parameter. The thickness of the ZrO_2 films was controlled by the deposition time, allowing the preparation of films which were 350~600 nm thick. The thickness and surface morphology of the flexible ZrO_2 films were measured by field-effect scanning electron microscopy (FESEM, Jeol, JSM-6700F) and atomic force microscopy (AFM, Digital Instruments, NanoScope). The structural properties and chemical states of the ZrO_2 films were examined by X-ray diffraction (XRD, PANalytical X'pert pro) and X-ray photoelectron spectroscopy (XPS, ULVAC-PHI, Quantera SXM), respectively. To measure the electrical properties of the ZrO_2 films, Al top electrodes 100 nm thick and 0.1~1 mm in diameter were deposited by DC sputtering, after which capacitors with an Al/ZrO_2/Al/PET structure were fabricated. The dielectric constant and dissipation factor were measured as a function of the frequency using an impedance-gain phase analyzer (HP 4194A). Leakage current-voltage (I-V) measurements were performed using a picoammeter (HP 4140B).

III. Results and Discussion

Fig. 1 shows XRD patterns of ZrO_2 films deposited on PET substrates at different sputtering pressures and gas ratios ($Ar:O_2$). The strong peak in the range of 20~30° was assigned to the semi-crystalline structure of the PET [4]. Apart from the strong PET peak, there are four ZrO_2 peaks at 30.05°, 35.13°, 50.43°, and 59.97°, which can be attributed to the (111), (200), (220), and (311) diffraction planes of the tetragonal ZrO_2. The peaks from the tetragonal ZrO_2 are clearly observed for the all films deposited at various pressures and gas ratios despite the fact these films are deposited at room temperature. According to the equilibrium phase diagram, bulk ZrO_2 shows three different crystalline structures of a

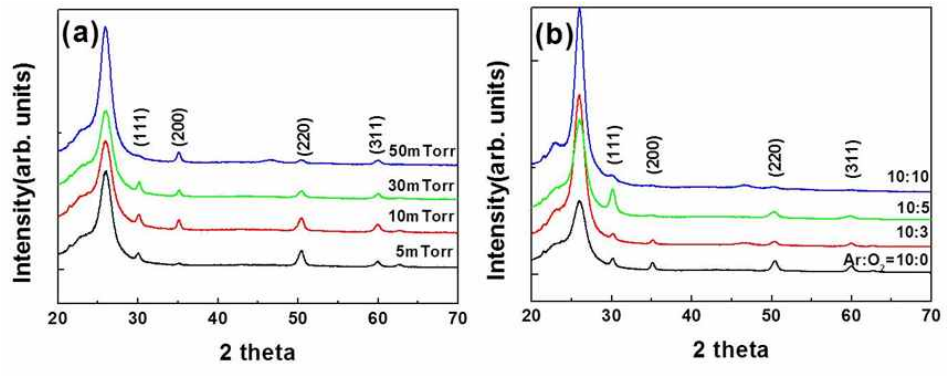

Figure 1. XRD patterns of ZrO_2 films deposited on PET substrates at different (a) sputtering pressures (Ar:O_2=1:0) and (b) Ar:O_2 gas ratios (10 mTorr)

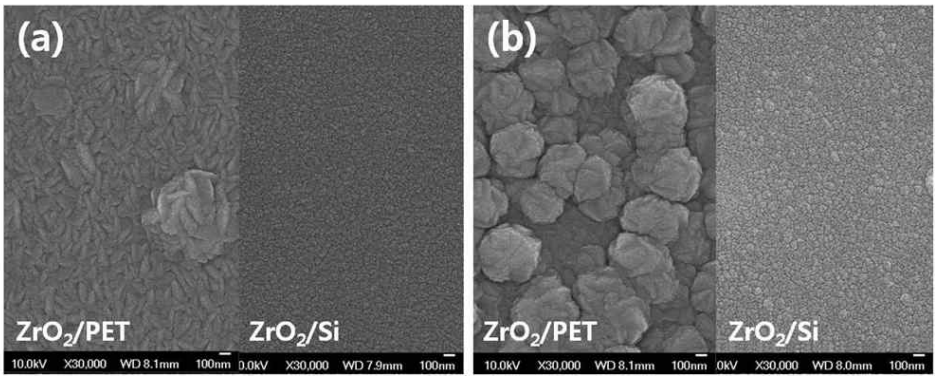

Figure 2. SEM surface images of ZrO_2 films deposited on PET and Si substrates as a function of the sputtering pressure: (a) 5 mTorr and (b) 50 mTorr (Ar:O_2=1:0)

monoclinic, a tetragonal and a cubic phase [14]. The formation of the tetragonal ZrO_2 film is considered to be a non-equilibrium formation process due to the deposition of high-energy sputtered particles. ZrO_2 films were deposited on Si substrates under identical deposition conditions in an effort to evaluate the substrate dependence on the crystal structure of the films. However, for the ZrO_2 films deposited on Si substrates at room temperature, no signals corresponding to crystalline ZrO_2 films could be observed in the XRD patterns. Fig. 2 shows SEM images of ZrO_2 films deposited on PET and Si substrates. Figs. 2(a) and (b) are images of films deposited at 5 and 50 mTorr, respectively. The films show the significant change of morphology with the substrate type. ZrO_2 films deposited on PET show large crystallites which are believed to be responsible for the formation of the crystalline peak in the XRD results. The precise reason for this requires further investigation.

Fig. 3 shows SEM surface images of ZrO_2 films grown on PET substrates at different pressure levels. The surfaces of all ZrO_2 films deposited at pressures ranging from 5 to 50 mTorr were relatively smooth and without defects such as cracks and pinholes as they were deposited at low temperatures. The inset of each image shows AFM images of films prepared at different pressures. The roughness of the films prepared at a low pressure is shown to be reduced compared to those of the films prepared at a high pressure. The surface roughness of the films increased with an increase in the sputtering pressure. The increase in the crystallite size can be explained in terms of the relationship between the mean-free path, λ (cm) and the sputtering pressure, as follows,

$$\lambda = 2.33\times10^{-20}\ T/(P\delta_n^2) \qquad (2)$$

where T(K) is the temperature, P(Pa) is the pressure and δ_n(cm) is the molecular diameter [15].

According to Eq. (2), the sputtered atoms undergo

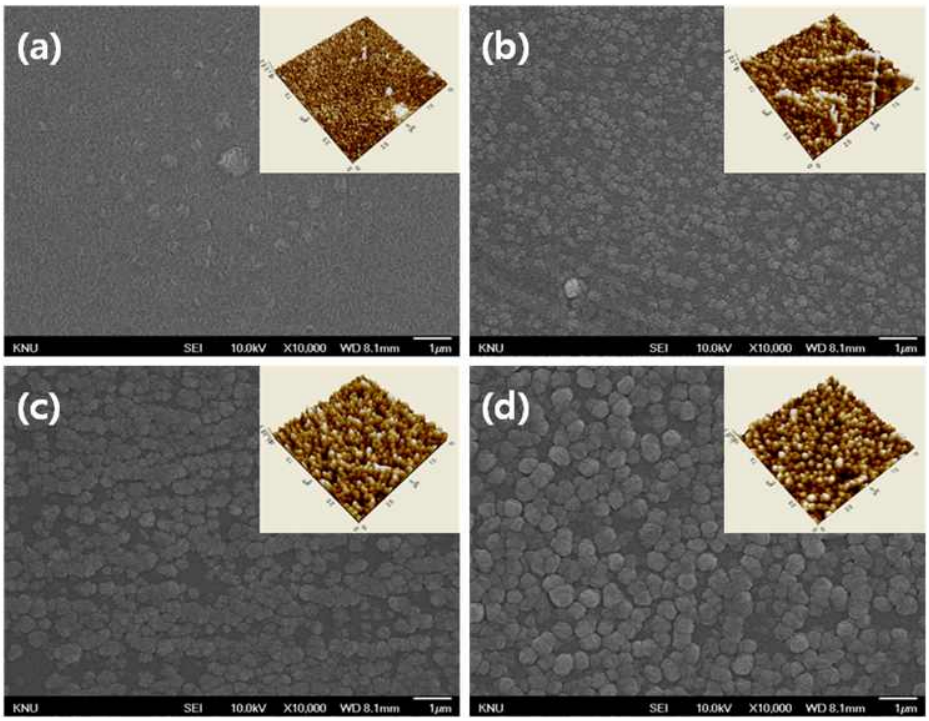

Figure 3. SEM surface images of ZrO_2 films deposited on PET substrates as a function of the sputtering pressure ($Ar:O_2$=1:0); (a) 5 mTorr, (b) 10 mTorr, (c) 30 mTorr and (d) 50 mTorr. Insets are AFM images of ZrO_2 films deposited under the same conditions.

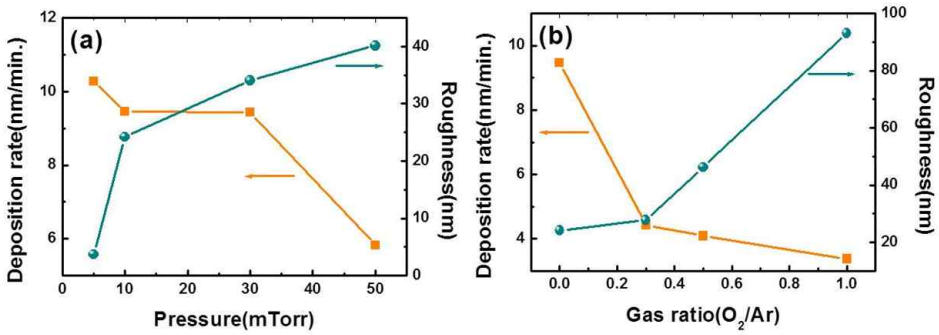

Figure 4. Deposition rate and roughness of ZrO_2 films prepared at different (a) sputtering pressures ($Ar:O_2$=1:0) and (b) gas ratios (10 mTorr).

a large number of collisions when the sputtering pressure is high, and they have a higher probability of agglomeration. Therefore, the crystallite size can increase before they arrive at the substrate surface.

Fig. 4(a) shows the deposition rate and roughness as a function of the sputtering pressure. The deposition rate of the films decreased with an increase in the sputtering pressure due to the decrease in the mean-free path [16,17]. The deposition rates of the films deposited at 5 and 50 mTorr were 10.3 and 5.8 nm/min, respectively. The decrease in the deposition rate with an increase in the pressure was attributed to collision scattering between the sputtered ZrO_2 and Ar species in the chamber. The RMS roughness of the films increased as the sputtering pressure increased. The ZrO_2 films showed a RMS roughness of 3.7 to 40 nm at a pressure ranging from 5 to 50 mTorr. This can be understood in terms of the following mechanism. The energy of the particles decreased with an increase in the pressure owing to the higher number of collisions. The surface mobility of the particles decreased with as the energy decreased [18]. Fig. 4(b) shows the deposition rate and roughness as a function of the gas ratio (O_2/Ar). The deposition rate of the films decreased with an increase in the gas ratio due to the decrease in sputtering efficiency

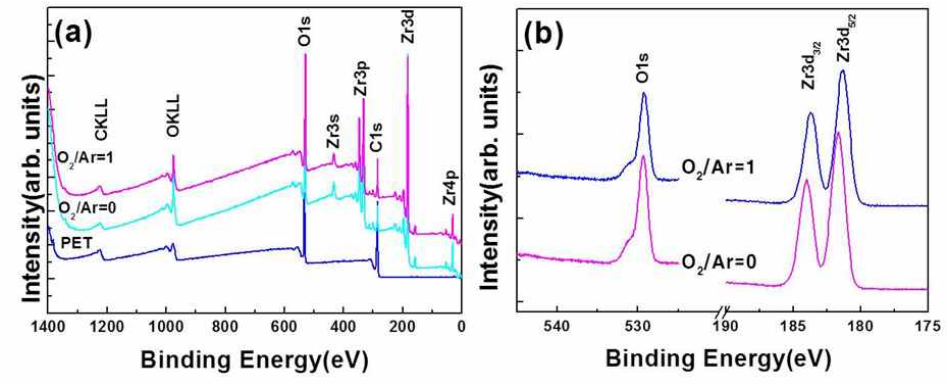

Figure 5. XPS spectra of (a) a wide-surface scan and (b) high-resolution scan obtained from ZrO_2 film deposited at 10 mTorr.

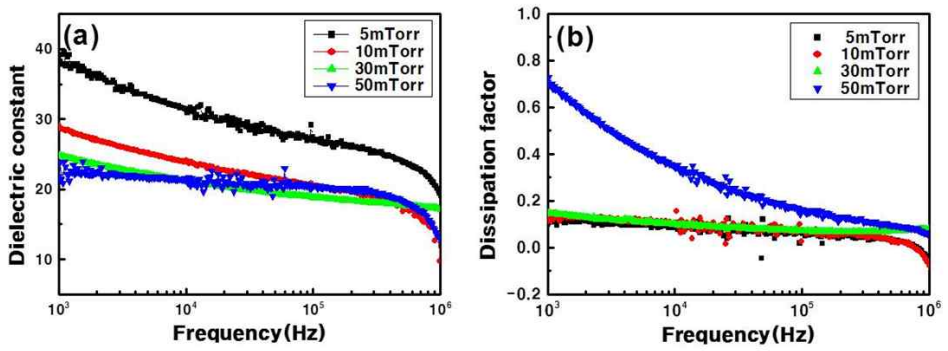

Figure 6. (a) Dielectric constant and (b) dissipation factor of ZrO_2 films deposited at a range of pressures.

as the oxygen partial pressure increased [19]. The deposition rates of the films deposited at gas ratios (O_2/Ar) of 0 and 1 were 9.4 and 3.3 nm/min, respectively. The RMS roughness of the films increased with an increase in the gas ratio. The ZrO_2 films showed a RMS roughness of 24.1 to 93 nm at gas ratios (O_2/Ar) ranging from 0 to 1. The surfaces of the film were became a surface with large white particles as the O_2/Ar gas ratio increased. As is well known, PET is quite sensitive to moisture and O_2 gas; hence, a PET substrate can absorb and become saturated with moisture and O_2 gas [20]. For this reason, the ZrO_2 films deposited in an O_2 gas atmosphere were considered to be unsuitable.

Fig. 5 shows the XPS spectra of the PET and ZrO_2 films deposited on PET substrates at different gas ratios. A monochromated Al k_α line and a constant energy of 280 eV were used in the experiments. All binding energies were calibrated at a binding energy of C1s (284.5 eV). In the wide scan shown in Fig. 5(a), the PET substrate shows a C1s peak at 284.5 eV, which was assigned to the CH group, as well as an O1s peak at 531.7 eV caused by residual carbon contamination. The Zr 3d peak appears at a binding energy (BE) of 182 eV and the 3d doublet splitting is 2.4 eV, which corresponds to ZrO_2. The surface compositions of the ZrO_2 films deposited at O_2/Ar ratios of 0 and 1 showed O/Zr ratios of 2.05 and 2.170, respectively. Fig. 5(b) shows the high- resolution XPS spectra of the Zr3d and O1s samples. The Zr $3d_{5/2}$ and Zr $3d_{3/2}$ peaks of the ZrO_2 films deposited at an O_2/Ar ratio of 0 were observed at 181.6 and 184.0 eV, respectively. The peaks for the films deposited at an O_2/Ar ratio of 1 were shifted to a lower binding energy by ~0.4 eV. This led to the formation of surface species with an oxidation state of Zr. ZrO_2 films deposited at an O_2/Ar ratio of 1 showed an opaque and white surface. There is also an O1s line at 529.1 eV,

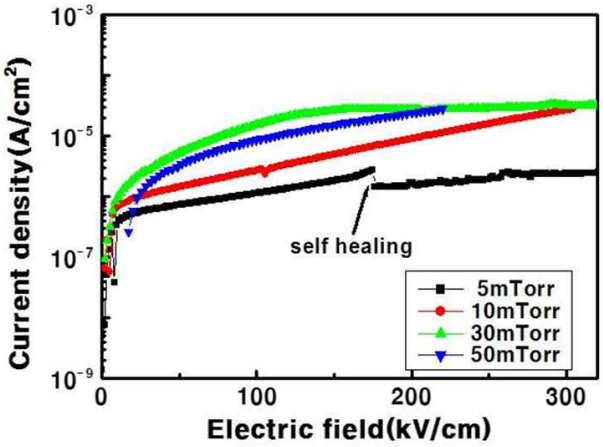

Figure 7. Leakage current density-electric field (J-E) curves of ZrO_2 films deposited at a range of pressures.

indicating the presence of surface OH- groups. These groups are always present when ZrO_2 is exposed to air. The oxygen-sufficient composition of ZrO_2 films can be attributed to the surface OH-groups.

To measure the electrical properties, ZrO_2 films were deposited in an Ar gas atmosphere. Figs. 6(a) and (b) show a change in the dielectric constant and the dissipation factor (tanδ) as a function of the frequency for ZrO_2 films deposited at different sputtering pressures. The dielectric constants of the ZrO_2 films decreased with an increase in the sputtering pressure. The films deposited at 5 to 50 mTorr showed a dielectric constant ranging from 21 to 38 at 1 kHz. These values are higher than those reported for monoclinic ZrO_2 films [21,22]. The effects of the sputtering pressure on the dissipation factor were negligible. The films deposited at 5 to 30 mTorr showed a dissipation factor of 0.09~0.14 at 1 kHz, whereas the film deposited at 50 mTorr showed a significantly high value of 0.7. In general, the microstructure of the thin films affects the dielectric constant and dissipation factor. From the SEM and AFM images shown in Fig. 3, it can be inferred that the high dissipation factor of the film deposited at 50 mTorr is due to the large crystallite size and rough surface. The dielectric constant of the films deposited at 5 mTorr was nearly twice that of the monoclinic ZrO_2 films and 7~12 times higher than those of polymer dielectrics such as PET and PP.

The leakage current in a high-energy-density capacitor should be as low as possible to optimize the storage capacity. Fig. 7 shows the leakage current characteristics of the ZrO_2 films. The leakage current increased gradually with an increase in the sputtering pressure. The leakage current was reported to be affected by the grain size, crystallinity and surface morphology [23]. The increase in the leakage current of the film with the sputtering pressure could be attributed to the increase in the surface roughness. The leakage current density of the ZrO_2 films was approximately 10^{-6}~10^{-5} A/cm^2 at 300 kV/cm. The film deposited at 5 mTorr showed fluctuation of the leakage current due to self-healing, which is the ability to recover after an instantaneous breakdown.

IV. Conclusions

This study examined the effects of the sputtering pressure and Ar:O_2 gas ratio as sputtering variables on the microstructure, surface morphology, deposition rate and electrical properties of ZrO_2 films. The sputtering pressure is the key deposition parameter affecting the electrical properties and the stable preparation of ZrO_2 films. Although they were prepared at room temperature, high-quality ZrO_2 films with a high dielectric constant and low leakage current could be obtained by controlling the sputtering pressure during the sputtering process. The ZrO_2 films prepared at 5 mTorr showed a dielectric constant of 38 at 1 kHz and a leakage current density of ~10^{-6} A/cm^2 at 300 kV/cm. This suggests that flexible ZrO_2 film prepared by sputtering can be a promising candidate for high-energy-density capacitors.

Acknowledgements

This study was supported by the Basic Science Research Program through the National Research Foundation of Korea (NRF) funded by the Ministry of Education, Science and Technology (No. 2012-0004538) and by the Kyungpook National University Research Fund of 2012.

References

[1] W. J. Sarjeant, J. Zirnheld, and F. W. MacDougall, IEEE Trans. Plasma Sci. **26,** 1368 (1998).

[2] M. T. Domonkos, S. Heidger, D. Brown, J. V. Parker, C. W. Gregg, K. Slenes, W. Hackenberger, S. Kwon, E. Loree, and T. Tran, IEEE Trans. Plasma Sci. **38,** 2686 (2010).

[3] J. L. Nash, Polymer Eng. Sci. **28,** 862 (1988).

[4] P. Karanja and R. Nath, IEEE Trans. Electr. Insul. **28,** 294 (1993).

[5] G. Love, J. Am. Ceram. Soc. **73,** 339 (1990).

[6] G. Brennecka, J. Ihlefeld, J-P. Maria, B. Tuttle, and P. Clem, J. Am. Ceram. Soc. **93,** 3935 (2010).

[7] P. Vitanov, A. Harizanova, T. Ivanova, Ch. Trapalis, and N. Todorova, Mat. Sci. Eng. B **165,** 178 (2009).

[8] N. Q. Minh, J. Am. Ceram. Soc. **76,** 563 (1993).

[9] M. Sayer and K. Sreenivas, Science **247,** 1056 (1990).

[10] A. P. Huang and Paul K. Chu, Mat. Sci. Eng. B **121,** 244 (2005).

[11] K. Galicka-Fau, C. Legros, M. Andrieux, M. Brunet, J. Szade, and G. Garry, Appl. Surf. Sci. **255,** 8986 (2009).

[12] W. T. Tang, Z. F. Ying, Z. G. Hu, W. W. Li, J. Sun, N. Xu, and J. D. Wu, Thin Solid Films **518,** 5442 (2010).

[13] S. Y. Bae, H. S. Choi, S. Y. Choi, and Y. J. Oh, Ceram. Int. **26,** 213 (2000).

[14] S. Ben Amor, B. Rogier, G. Baud, M. Jacquet, and M. Nardin, Mat. Sci. Eng. B **57,** 28 (1998).

[15] L. I. Maissel and R. Glang, *Handbook of Thin Film Technology* (McGraw-Hill Inc. New York, USA, 1970), p. 22.

[16] T. Minami, S. Ida, and T. Miyata, Thin Solid Films **416,** 93 (2002).

[17] V. Assuncao, E. Fortunato, A. Marques, H. Aguas, I. Ferreira, M. E. V. Costa, and R. Martins, Thin Solid Films **427,** 401 (2003).

[18] P. Zeman and S. Takabayashi, Surf. Coat. Technol. **153,** 93 (2002).

[19] R. F. Bunshah, *Handbook of Deposition Technologies for Films and Coatings* (2nd ed. Noyes Publication, USA, 1994), p. 270.

[20] S. K. Park, J. I. Han, W. K. Kim, and M. G. Kwak, Thin Solid Films **397,** 49 (2001).

[21] C. Y. Ma, F. Lapostolle, P. Briois, and Q. Y. Zhang, Appl. Surf. Sci. **253,** 8718 (2007).

[22] P. Y. Kuei, J. D. Chou, C. T. Huang, H. H. Ko, and S. C. Su, J. Cryst. Growth **314,** 81 (2011).

[23] Y. B. Chen and C. L. Huang, Surf. Coat. Technol. **201,** 643 (2006).